Geological and Atmospheric Sciences Publications   Geological and Atmospheric Sciences

2002

Toward improved prediction of mesoscale convective system dissipation

Joseph J. Gale
Iowa State University

William A. Gallus Jr.
Iowa State University, wgallus@iastate.edu

Karl A. Jungbluth
National Weather Service Forecast Office

Toward improved prediction of mesoscale convective system dissipation

Abstract

The complex issue of mesoscale convective system (MCS) dissipation over the central United States is investigated using both observations and Eta Model output from 47 cases that occurred during May-August 1998-99 in Iowa and surrounding states. The cold pool-shear balance theory of Rotunno et al. and Weisman, through tests with observational data, is not found to correlate well with actual dissipation of these MCSs. Differences are discussed that may account for the discrepancies between the results of the present study and the cold pool-shear balance theory. Both surface (SSRI) and elevated (ESRI) system-relative inflow tend to decrease as the MCSs near dissipation, due in part to a decrease in MCS speed of movement. A low-level jet (LLJ) affects most of the MCSs at some time during their life cycles, and there is a tendency for MCSs that were once affected by an LLJ to dissipate once no longer affected by an LLJ. A few cases experience significant decreases in the 850-500- and 700-500-mb lapse rates just prior to dissipation, indicating MCS movement into more stable environments. Maximum 0-2-km equivalent potential temperature decreases during the life cycle, but most often from a very high value to a moderate value that still implies adequate energy for the MCSs. To determine the best model predictors of MCS dissipation, many parameters are examined from the Eta Model. Among these, only a decrease in the 850-mb equivalent potential temperature advection may be a potential predictor of MCS dissipation.

Keywords

climate change, environmental engineering, stable environments, weather forecasting, convective system, dissipation, mesoscale meteorology, United States

Disciplines

Atmospheric Sciences | Geology | Meteorology

Toward Improved Prediction of Mesoscale Convective System Dissipation

JOSEPH J. GALE AND WILLIAM A. GALLUS JR.

Iowa State University, Ames, Iowa

KARL A. JUNGBLUTH

National Weather Service Forecast Office, Johnston, Iowa

ABSTRACT

The complex issue of mesoscale convective system (MCS) dissipation over the central United States is investigated using both observations and Eta Model output from 47 cases that occurred during May–August 1998–99 in Iowa and surrounding states. The cold pool–shear balance theory of Rotunno et al. and Weisman, through tests with observational data, is not found to correlate well with actual dissipation of these MCSs. Differences are discussed that may account for the discrepancies between the results of the present study and the cold pool–shear balance theory. Both surface (SSRI) and elevated (ESRI) system-relative inflow tend to decrease as the MCSs near dissipation, due in part to a decrease in MCS speed of movement. A low-level jet (LLJ) affects most of the MCSs at some time during their life cycles, and there is a tendency for MCSs that were once affected by an LLJ to dissipate once no longer affected by an LLJ. A few cases experience significant decreases in the 850–500- and 700–500-mb lapse rates just prior to dissipation, indicating MCS movement into more stable environments. Maximum 0–2-km equivalent potential temperature decreases during the life cycle, but most often from a very high value to a moderate value that still implies adequate energy for the MCSs. To determine the best model predictors of MCS dissipation, many parameters are examined from the Eta Model. Among these, only a decrease in the 850-mb equivalent potential temperature advection may be a potential predictor of MCS dissipation.

1. Introduction

Mesoscale convective systems (MCSs) are common occurrences during spring and summer over the central United States. Previous studies have documented mesoscale convective complexes (MCCs) (Maddox 1980), a subset of MCSs that are long lived; exhibit large, quasi-circular cold cloud shields in infrared (IR) satellite imagery; and are predominantly nocturnal. MCCs are important to the water needs of the central plains because of their contribution to summertime rainfall over that region. In particular, Fritsch et al. (1986) concluded that MCCs could account for 20%–50% of annual rainfall over a broad region of the central plains states, with June–August precipitation being particularly dominated by MCCs.

Annual summaries of MCC occurrences over the United States (Maddox 1980; Maddox et al. 1982; Rodgers et al. 1983, 1985; Augustine and Howard 1988, 1991; Anderson and Arritt 1998) have shown that, in addition to the ample rainfall, MCCs are also associated with a high frequency of severe weather, including tornadoes, hail, high winds, and flash floods. Accurate forecasting of MCCs, and thus, MCSs, is imperative because of the high frequency of severe weather and large percentage of summertime rainfall attributed to them.

MCS dissipation has a direct impact not only on severe weather forecasting but also on cloud trend and maximum temperature forecasts (Maddox and Heckman 1982). Some simple guidance was provided by McAnelly and Cotton (1989) that might help in predicting large-scale dissipation trends. They noted MCCs would end on average about 4 h after the maximum coverage or coldness of the cloud top had been achieved. In general, however, prediction of MCS dissipation has not been addressed in the literature. The focus of MCS studies has instead usually been on prediction of the formation of MCSs. The studies of Rotunno et al. (1988) and Weisman (1992) are important, because they are two studies that discuss possible causes of MCS dissipation.

Rotunno et al. (1988) modeled strong, long-lived squall lines, and their results suggested that the balance between the ambient low-level line-normal shear circulation and the opposing evaporation-induced surface cold pool circulation determined the strength and struc-

Corresponding author address: William A. Gallus Jr., Dept. of Geological and Atmospheric Science, Iowa State University, 3010 Agronomy Hall, Ames, IA 50011.
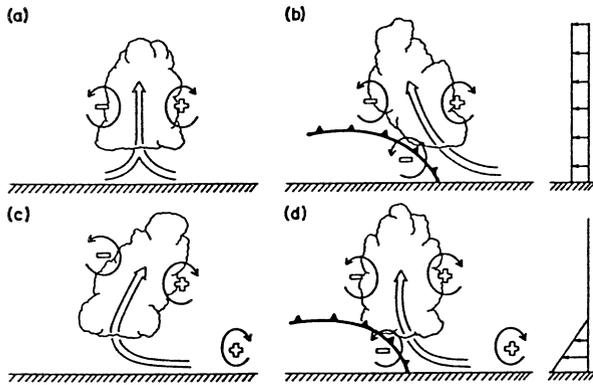E-mail: wgallus@iastate.edu

FIG. 1. Schematic diagram showing how a buoyant updraft may be influenced by line-normal vertical wind shear and/or a cold pool. (a) With no shear and no cold pool, the axis of the updraft produced by the thermally created, symmetric vorticity distribution is vertical. (b) With a cold pool, the distribution is biased by the negative vorticity of the underlying cold pool and causes the updraft to tilt upshear. (c) With shear, the distribution is biased toward positive vorticity causing the updraft to tilt downshear. (d) With both a cold pool and shear, the two effects may negate each other, and allow an erect updraft. [Adapted from Fig. 18 of Rotunno et al. (1988).]

ture of long-lived squall lines. If one circulation overpowered the other, the system weakened and eventually dissipated (Fig. 1).

Similarly, Weisman (1992) theorized that once the cold pool circulation had begun to overwhelm the ambient low-level line-normal shear circulation, if a rear-inflow jet (Smull and Houze 1987) descended to the surface, it would further strengthen the cold pool circulation and cause faster dissipation. If a rear-inflow jet remained elevated, it would induce a circulation below it opposite the cold pool's circulation, thus aiding the ambient line-normal low-level shear circulation and extending the MCS's lifetime.

Other studies briefly suggest possible reasons for MCS dissipation. Parker and Johnson (2000) found that for one particular MCS, a pocket of enhanced lower-tropospheric equivalent potential temperature θ_e might have provided fuel for the development of the MCS. When dry, lower-θ_e air moved in from the west 5 h after the MCS had begun to develop, the MCS began to dissipate. Also, Cotton et al. (1989) found that an elevated layer from 900 to 700 mb of high-θ_e values was important in sustaining MCCs. This suggests low-level θ_e is worthy of study as a potential predictor of MCS dissipation.

Another parameter that may have an effect on the dissipation of MCSs is the low-level jet (LLJ). Many previous studies have documented the nocturnal LLJ as an important factor in the development of MCSs over the Great Plains (e.g., Augustine and Caracena 1994; Mitchell et al. 1995; Arritt et al. 1997; Anderson and Arritt 1998). The LLJ has been shown to supply warm, moist air into the Great Plains to aid in the development of MCCs (Maddox 1980; Cotton et al. 1989; Augustine

and Howard 1991), and it also increases convergence at the nose of the jet axis (Bonner 1968).

In particular, Augustine and Howard (1991) found that a well-defined mean LLJ over the Great Plains was present during active-MCC periods (periods of several weeks during which MCCs occurred frequently), but it was not present during null-MCC periods (periods of several weeks during which MCCs occurred infrequently). The LLJs advected moisture from the Gulf of Mexico as far north as the northern plains to contribute to the formation and sustenance of MCCs. MCCs moved in a general easterly direction as they matured and, thus, eventually moved east of the region of maximum occurrence of LLJs—northern Texas through southern Nebraska (Mitchell et al. 1995)—and the moisture and convergence supplied by them. Though there is an established link between the LLJ and MCS development, it is uncertain what role the LLJ plays in the dissipation of MCSs.

In the present study, we examine observations and model output to determine potential predictors of MCS dissipation. Most of the MCSs we studied exhibited some degree of linear structure, allowing us to test the cold pool circulation versus ambient low-level line-normal shear circulation theory of Rotunno et al. (1988) with observations. We use both observations and/or model output to study low-level θ_e, the LLJ, surface and elevated system-relative inflow, and other parameters that may potentially influence MCS dissipation.

2. Data and methodology

Observations and model output were analyzed from 47 cases that occurred during May–August 1998–99. Cases were limited to those occurring in Iowa or surrounding states since this project was conducted in collaboration with the National Weather Service Forecast Office in Johnston, Iowa. Cases were also limited to nocturnal MCSs since it is the late night through afternoon dissipation of these systems that most challenges forecasters.

Next-Generation Weather Radar (NEXRAD) National Mosaic Reflectivity Images archived by the National Climatic Data Center (NCDC) were used to find nocturnal MCS cases and to document their evolution. No specific size criteria were required to classify areas of precipitation as MCSs for the present study. However, the duration of the MCSs had to be at least 6 h and the MCSs had to be ongoing for at least 1 h during the 0600–1800 UTC time period for which observational data were analyzed. The time of initiation was defined to be the hour in which the first convective cells developed that would eventually evolve into an MCS. An MCS was defined to have dissipated when all convective and/or heavy stratiform echoes (reflectivity >35 dBZ) were no longer present, and when, at most, only light stratiform precipitation (reflectivity ≤35 dBZ) remained. In accordance with Cotton et al. (1989), the

study emphasized MCSs, which evolved in mostly barotropic environments apart from strong dynamic forcing. MCSs that evolve in barotropic environments provide greater challenges to midwestern National Weather Service forecasters than MCSs that evolve in baroclinic environments because it is more difficult to determine when and where the MCSs will form and subsequently dissipate, or how severe the MCSs will become. Numerical weather prediction models also tend to have worse forecasts for barotropic MCSs (Stensrud et al. 2000).

a. Observational data

Observational data were analyzed at 0600, 1200, 1500, and 1800 UTC. Parameters calculated using the observational data included cold pool strength; surface system-relative inflow; elevated system-relative inflow; maximum 0–2-km above ground level (AGL) wind; 0–1-, 0–2-, and 0–3-km line-normal shear; low-level jet, lapse rates (surface–700 mb, 850–500 mb, 700–500 mb); and maximum 0–2-km AGL θ_e. Lapse rates and maximum 0–2-km θ_e were computed only at 0000 and 1200 UTC. A variety of data sources were utilized to compute these parameters, including surface observations, the wind profiler network, rawinsonde observations, and NEXRAD National Mosaic Reflectivity Images.

1) COLD POOL STRENGTH

Cold pool strength was computed by first determining the buoyancy gradient as a surface temperature difference between the coldest temperature found in the cold pool and the average temperature of the ambient environment immediately ahead of the system. Similarly, a pressure perturbation was then computed between the cold pool and the ambient environment immediately ahead of the system. To estimate the depth of the cold pool, the pressure perturbation was input into the cold pool initialization scheme of Stensrud et al. (1999) along with rawinsonde observations from a representative site within 300 km ahead of the system. Once these parameters were computed, the cold pool strength was calculated and compared to the line-normal shear to test the circulation balance theory of Rotunno et al. (1988).

Weisman (1992) expressed the cold pool–shear balance relationship developed by Rotunno et al. (1988) quantitatively in the form of a ratio $C/\Delta u$, where C represents the cold pool strength and Δu represents the velocity difference between the surface and 2.5 km AGL in the ambient air ahead of the cold pool. Weisman (1992) defined C via

$$C^2 = 2 \int_0^H (-B) \, dz, \qquad (1)$$

where B represents the buoyancy, defined as

$$B \equiv g \left[\frac{\theta'}{\overline{\theta}} + 0.61(q_v - \overline{q}_v) - q_c - q_r \right], \qquad (2)$$

and where θ is the potential temperature and q_v, q_c, and q_r are the mixing ratios of water vapor, cloud water, and rainwater, respectively. Bars over θ and q_v represent environmental values of potential temperature and water vapor mixing ratio, respectively. The integral is calculated through the depth of the cold pool (H) at a representative location behind the cold pool nose (i.e., avoiding the region of internally enhanced cold pool depth right at the leading edge) and describes the kinetic energy consumed by lifting a parcel through depth H.

For the present study, the buoyancy parameter B could not be calculated precisely as in Weisman (1992) because of the unavailability of data to calculate the mixing ratios of cloud water and rainwater. Therefore, it was estimated via

$$B = g \left[\frac{(T_c - T_a)}{T_a} \right], \qquad (3)$$

where T_c is the coldest surface temperature found in the cold pool and T_a is the average ambient surface temperature immediately ahead of the system. The expression $|T_c - T_a|$ is referred to as the buoyancy gradient. This measure of buoyancy is similar to Weisman (1992). For simplicity, a surface temperature perturbation between the cold pool and the environment was used instead of a potential temperature perturbation. A scale analysis showed that the mixing ratios of water vapor, cloud water, and rainwater would roughly be an order of magnitude smaller than the perturbation temperature term, so that their neglect from B should not result in significant differences from Weisman (1992).

Once B was calculated, it was substituted into Eq. (1). Then it was integrated over the calculated cold pool depth to yield a value for C. Since it would be nearly impossible to know T_a above the surface with conventional observations, we chose to hold B constant throughout the cold pool depth. A sensitivity test was performed for which B was permitted to vary with height, using the output from the Stensrud et al. (1999) cold pool initialization scheme. Because many of our events were evaluated at times when ambient low-level stability was large, changes in C resulting from the use of a vertically varying B were negligible, supporting our use of the constant value, easily computed from surface observations.

Once C was calculated, it was compared with the line-normal shear values. However, unlike Weisman (1992) who used only line-normal shear from 0 to 2.5 km AGL, line-normal shear was calculated for three layers: 0–1, 0–2, and 0–3 km. The layer agreeing most closely with the estimated cold pool depth was used in the comparison.

2) LINE-NORMAL SHEAR

The line-normal vertical wind shear was computed using wind profiler observations and surface observations. To compute the 0–2-km vertical wind shear, for example, a wind profiler site was chosen that was representative of the environment within 300 km ahead of the MCS. Then the surface wind vector closest to the wind profiler site was subtracted from the wind vector at 2 km to result in the 0–2-km vertical wind shear. Line-normal shear was then computed for those MCSs that were exhibiting linear convective modes at the observation time. The majority of MCSs studied exhibited linear convective modes for a significant amount of their duration.

3) SURFACE AND ELEVATED SYSTEM-RELATIVE INFLOW

Surface system-relative inflow (SSRI) and elevated system-relative inflow (ESRI) were also computed, requiring the calculation of the MCS motion vector. The MCS motion vector was subtracted from average ground-relative surface winds (resulting in SSRI) or maximum 0–2-km winds (resulting in ESRI) from representative environments ahead of the MCS. ESRI was computed in addition to SSRI because the majority of the MCSs studied were north of a boundary, and thus, the convection was likely elevated and drawing more of its inflow from levels above the surface than from the surface itself. In addition, low-level nocturnal inversions were also present at 1200 UTC for most MCS environments. NEXRAD National Mosaic Reflectivity Images were used to track MCS movement, surface observations were used to compute ground-relative surface winds (hereinafter surface winds), and wind profiler observations were used to compute maximum 0–2-km winds.

Plots of each MCS track were made in order to calculate the MCS motion vector. For times when convection was ongoing within the MCS, the track was plotted in terms of the position of the center of the convection. For example, most of the MCSs studied developed linear configurations in their convective echoes. At these times, the MCS position was plotted as the position of the center of the convective line. For times when no convection was ongoing within the MCS, the track was plotted in terms of the position of the center of the stratiform rain area of the MCS. To calculate the motion vector of an MCS at 1200 UTC, the position of the MCS was plotted for 1 h before and 1 h after 1200 UTC. This allowed the computation of an average MCS motion vector for 1200 UTC. If convection were present for only a portion of the 1100–1300 UTC period, the position of the center of the stratiform rain area was used to plot the MCS track for the full 2 h.

4) LOW-LEVEL JET

Wind profiler data were used to calculate the occurrence of LLJs for each wind profiler station on an hourly basis. The criteria used to define LLJ occurrences are those of Bonner's (1968) study that require a low-level, local maximum (between the 500- and 3000-m levels) in the vertical profile of the horizontal wind speed. A criterion-1 LLJ has a speed maximum of at least 12 m s^{-1} that must decrease by at least 6 m s^{-1} both above (before surpassing the 3000-m level) and below the speed maximum. Similarly, a criterion-2 LLJ has a speed maximum of at least 16 m s^{-1} that must decrease by at least 8 m s^{-1}, and a criterion-3 LLJ has a speed maximum of at least 20 m s^{-1} that must decrease by at least 10 m s^{-1}.

Under these classifications, a criterion-3 LLJ can also be classified as a criterion-2 and a criterion-1 LLJ, and a criterion-2 LLJ can also be classified as a criterion-1 LLJ. Thus, all LLJs can be classified as criterion-1 LLJs. However, consistent with Mitchell et al. (1995) and Arritt et al. (1997), the present study considers the criteria in a nonoverlapping sense in order to gauge possible differences between strong and weak LLJs in regard to MCS dissipation. It has been established in previous research (e.g., Arritt et al. 1997) that the direction of the LLJ is typically from the south or southwest in the central and southern Great Plains. Wind profiler data were examined from sites ahead of or in representative environments to the south or southwest of the MCS to determine if a particular MCS was being affected by an LLJ at a certain time. The LLJ also had to be within a 300-km radius of the MCS to be defined as likely affecting the MCS in some way.

The LLJ data are available for the months of June–August of 1998–99. Therefore, since May data were unavailable, the LLJ dataset was limited to 37 MCSs instead of 47.

5) LAPSE RATES AND MAXIMUM 0–2-KM θ_e

Lapse rates and maximum 0–2-km θ_e were calculated using rawinsonde observations and surface observations at 0000 and 1200 UTC from representative sites in environments within 300 km ahead of the MCS. Lapse rates were computed for three layers: surface–700 mb, 850–500 mb, and 700–500 mb.

b. Eta Model output

In order to determine the best model predictors of MCS dissipation, many parameters were examined from the National Centers for Environmental Prediction's (NCEP) Eta Model output [details of the Eta Model can be found in Mesinger et al. (1988) and Janjic (1994)]. Parameters examined include wind speed, convergence, moisture convergence, frontogenesis, θ_e, and θ_e advection at 850 mb for all, 500-mb vorticity advection, and

250-mb divergence. Eta Model output for Eta-generated MCSs was examined at 0600 and 1200 UTC for MCSs that appeared to weaken substantially or dissipate before 1800 UTC, and 1200 and 1800 UTC for MCSs that dissipated after 1800 UTC. To gauge MCS dissipation in the Eta Model, 6-h accumulated precipitation output was analyzed. Once the Eta stopped or substantially decreased the precipitation associated with the MCS, the MCS was deemed to have weakened substantially or dissipated. The 0000 UTC Eta Model output was used whenever possible, but since forecasters usually do not have access to the 0000 UTC run until after 0300 UTC, the earlier 1200 UTC Eta Model run was used when observed MCSs were ongoing before 0300 UTC. As will be discussed later, the average time of initiation of the MCSs is 0000 UTC, but more MCSs initiated before 0000 UTC than after 0000 UTC.

The maximum value shown by the Eta Model was recorded for each parameter. This value had to be within 300 km of the Eta-generated MCS's position, not the position of the observed MCS. The Eta-generated MCS's position was used in order to better understand how certain parameters within the Eta Model influence its MCSs. The Eta-generated MCS's position was sometimes a significant distance from the position of the observed MCS, but a thorough analysis of model spatial errors is beyond the scope of the present study.

3. Results

The 47-case dataset analyzed using observational data depicts the broad range of behaviors exhibited by MCSs. Before discussing results of the specific parameters computed, it is prudent to describe some general characteristics of the dataset as a whole.

One characteristic that over 90% of the MCSs exhibited was linear convective echo patterns for at least a small portion of their duration, with the majority exhibiting persistent (over one-half their lifetimes) linear convective patterns.

Even though all cases were nocturnal, the time of initiation, time of dissipation, and duration of the cases varied markedly. Still, nearly 80% initiated between 2000 and 0500 UTC (midafternoon and midnight local time), with an average initiation time of 0000 UTC. A common area of initiation was east of the Rocky Mountains in the Great Plains. Convection often initiated there in the mid- to late afternoon and early evening, organized into an MCS during the evening, and proceeded eastward overnight into the morning hours, possibly curving southeast as well. This corresponds well to results reported in MCC annual summaries (Maddox 1980; Maddox et al. 1982; Rodgers et al. 1983, 1985; Augustine and Howard 1988, 1991; Anderson and Arritt 1998).

The average time of dissipation was 1900 UTC, or early afternoon local time, with more cases dissipating before 1900 UTC than after. Although the average du-

ration of the MCSs was 19 h, the wide range of initiation and dissipation times led to a wide range of duration, from 8 to 30 h.

The position of MCSs in relation to boundaries was also examined. Twenty-seven of the MCSs occurred north of a boundary (stationary front, warm front, or an outflow boundary). Twenty MCSs occurred in the warm sector, either south or east of a boundary. The propensity for these MCSs to develop north of a boundary implies the majority of the convection associated with them is elevated since inflow air with a southerly component likely has to rise over the boundary to be ingested into the system. However, the 20 cases that were in the warm sector may have exhibited predominantly surface-based convection, thus adding even more variability to the MCS dataset. Warm sector cases also at times may have exhibited elevated convection when a nocturnal low-level temperature inversion formed, creating a stable layer near the surface. Low-level temperature inversions were present for almost all examined 1200 UTC soundings.

It is noted that MCSs north of boundaries last 3 h longer, on average, with later mean dissipation times than MCSs in the warm sector. MCSs north of boundaries initiate at 0000 UTC and dissipate at 2000 UTC on average, while warm sector cases initiate at 2300 UTC and dissipate at 1600 UTC.

a. Cold pool–shear balance ratio

Rotunno et al. (1988) and Weisman (1992) theorized that one of the most important factors in the development and sustenance of the strongest, longest-lived squall lines is a vorticity balance. The horizontal vorticity associated with the squall lines' cold pools balances the horizontal vorticity from ambient low-level line-normal shear such that erect updrafts of convective cells are maintained. Recall that the cold pool–shear balance ratio is represented by $C/\Delta u$, where C represents the cold pool strength as defined in Eqs. (1) and (3), and Δu represents the ambient line-normal shear in the cold pool layer. The main components of C are the buoyancy gradient, $|T_c - T_a|$, from Eq. (3), and the estimated cold pool depth.

1) BUOYANCY GRADIENT–COLD POOL STRENGTH

Buoyancy gradient calculations show an average buoyancy gradient of 4.3 K for all times and all cases. This value of 4.3 K is within the range of a special set of cold pool simulations initialized by Rotunno et al. (1988) with a potential temperature perturbation decreasing linearly with height from 6 to 3 K from the surface to 1 km (note that those special simulations were separate from their primary squall line simulations, which were initialized with warm bubbles).

An examination of changes in the buoyancy gradient with time shows that, on average, it is weakest at 1200
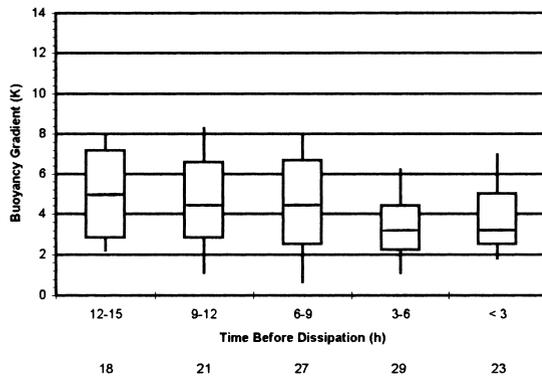
FIG. 2. Box and whiskers plot of buoyancy gradient (K) with time before dissipation (h). Boxes denote the 25th–75th percentiles, and vertical lines (whiskers) extend to the 10th and 90th percentiles. Horizontal bars within the boxes denote median values. The sample size for each 3-h bin is shown below the x-axis label.

FIG. 3. As in Fig. 2 but for line-normal shear (m s⁻¹).

UTC and strongest at 1800 UTC (figure not shown). The average temperature in the cold pool varies less than 1 K between all four times, hovering between 291 and 292 K. Therefore, it must be changes in the average environmental temperature, primarily from diurnal effects, that dictate changes in the buoyancy gradient.

It is useful to examine the results in terms of time before dissipation in addition to time of day. At 1200 UTC, for example, many cases were halfway through their life cycle, while others were near dissipation or just initiating. Examining results solely in terms of time of day would therefore make it difficult to determine which parameters are potential predictors of dissipation. The data have been divided into subsections of 3-h periods since calculations of parameters were made 3 or 6 h apart. Henceforth, results of the parameters studied will be shown primarily in terms of time before dissipation.

The average buoyancy gradient changes little as the MCSs approach dissipation (Fig. 2). Figure 2 is the first of many box and whisker plots to come. The boxes stretch from the 25th to 75th percentiles, and the thin vertical lines (whiskers) extend to the 10th and 90th percentiles. The thick horizontal bar in each box denotes the median. In addition, the sample size for each 3-h bin is shown below the x-axis label. It is evident that the buoyancy gradient changes little as dissipation approaches, with slightly lower values common close to dissipation.

As would be expected, an analysis of the cold pool strength itself (not shown) finds the same trends as the buoyancy gradient. It is lowest at 1200 UTC at 10.5 m s⁻¹, and highest at 1800 UTC at 21.0 m s⁻¹. Note the units are meters per second because the cold pool strength is being expressed as the wind speed the low-level flow maintains while being turned and lifted vertically the depth of the cold pool (Rotunno et al. 1988). The trend with time before dissipation is also the same, with the average values of C being greatest 12–15 h
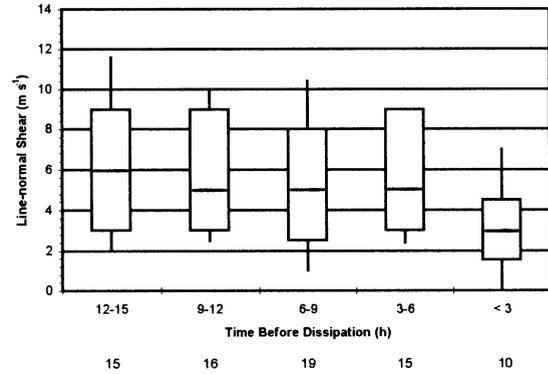
before dissipation and then decreasing slightly as dissipation nears.

A brief analysis of the estimated cold pool depth shows nearly one-half of the cases experienced very little change in the cold pool depth as time went on. The cold pool depth values range from near 0 to near 2 km, but they average near 1 km for each time period.

2) LINE-NORMAL SHEAR

The line-normal shear follows a trend similar to the buoyancy gradient. Figure 3 shows line-normal shear is fairly steady as the MCS progresses, except less than 3 h before dissipation when there is a notable decrease. At first glance, this decrease appears significant (the difference between the means of the 3–6-h bin and the <3 h bin are significant at the 95% confidence level), but there is a lot of variability in the dataset, and the MCSs with low values of line-normal shear less than 3 h before dissipation typically exhibited low values of line-normal shear throughout their life cycles.

3) COLD POOL–SHEAR BALANCE RATIO

The cold pool–shear balance ratio, expressed as $C/\Delta u$ for the cases in the present study, averages 3.8 for all cases and times combined. This is in contrast to Weisman's (1992) 4-h simulations, which did not yield a cold pool–shear balance ratio of greater than 1.6 at any time for either the moderate-shear (0–2.5-km shear of 15 m s⁻¹) or strong-shear (0–2.5-km shear of 25 m s⁻¹) simulations. However, the results are a bit closer to Weisman et al. (1988), whose simulations with 0–2.5-km shear of 10 m s⁻¹ yielded cold pool–shear balance ratios between 2 and 2.5.

Examination of the results in terms of time before dissipation (Fig. 4) shows that the cold pool–shear balance ratio is generally highest early on and lower as dissipation approaches, opposite what the cold pool–shear balance theory suggests. A discussion of reasons why the theory may not work well at predicting MCS dissipation follows in the next section.
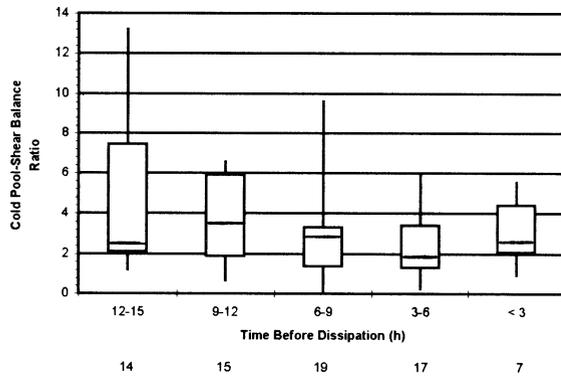
Fig. 4. As in Fig. 2 but for the cold pool–shear balance ratio.

It should be noted that the simulations in Weisman (1992) assumed surface-based convection, so the cases in the present study were separated in order to determine whether the warm sector cases exhibited cold pool–shear balance results that would agree more with the cold pool-shear balance theory. Unfortunately, this partitioning reduces the number of measurements per subsection significantly (sometimes less than five) for warm sector cases (figure not shown), so that an assessment cannot be made.

4) Discussion

There are several differences between Weisman's (1992) simulations and the MCSs of the present study. The largest may be the difference between Weisman's 0–2.5-km shear and the low-level line-normal shear values observed for the present study. The average line-normal shear in the present study for all times and cases combined is 5.6 m s^{-1}. Weisman used a moderate-shear value of 15 m s^{-1} and a strong-shear value of 25 m s^{-1}, values much higher than observed for the present study's cases. In fact, out of 93 measurements of line-normal shear, only 1 has a value of 15 m s^{-1}, and there are no higher values. Thus, the average line-normal shear for the present study is roughly one-third that used in Weisman's moderate-shear simulation. In addition, Weisman's cold pool–shear balance ratio numbers for the moderate-shear simulation range from 1.3 to 1.6, close to one-third the average balance ratio number in the present study.

The low values of shear in the present study are generally not due to the use of the cold pool depth (i.e., 0–2 km) instead of 2.5 km. In some cases, however, the 0–2.5-km shear would have yielded values several meters per second different from the shear over the cold pool depth, but the different values would be both higher sometimes and lower sometimes and likely average out.

One reason why Weisman's (1992) low-level shear values must be so large to balance the cold pool circulation and keep updrafts erect could be because his simulations have constant winds above the 2.5-km level.

Perhaps if midlevel and upper-level shear were included in the simulations, the low-level shear would not have to be as large to keep the MCS updrafts erect. Coniglio and Stensrud (2001) modeled a progressive derecho event allowing for mid- and upper-level shear and found 0–2.5-km shear values around 11 m s^{-1}, yet strong convective updrafts were periodically generated above the gust front for over 6 h and did not become weaker with time. Weisman et al. (1988) ran simulations of 10 m s^{-1} shear confined to 0–2.5 km and found a squall line ceased significant cell regeneration after 2 h. The results of Coniglio and Stensrud (2001) suggest that even if the cold pool circulation overwhelms the low-level shear, squall lines can maintain their strength for long periods if deep-tropospheric shear is sufficient.

Weisman and Rotunno (2001) have recently noted that a better application of the cold pool–shear balance theory may be to consider shear over a deeper layer, such as 0–5 km. They note that optimal systems tend to have a ratio between 1 and 1.5 (somewhat weaker ambient shear in comparison with the cold pool circulation), and that a wider range of environments outside the "optimal" state supports significant, long-lived squall lines in their newer simulations.

Deep-tropospheric shear (line normal) was examined for 10 MCSs of the present study from 0–5 and 0–9 km. The deep-tropospheric line-normal shear values are large enough to suggest that winds above the lowest few kilometers are generally not uniform. However, there is much variability even among the 10 MCSs studied in this subset. For 0–5-km shear for example, several MCSs experienced deep-tropospheric shear much greater than 10 m s^{-1}; for others, shear was less than 5 m s^{-1}.

Coniglio and Stensrud (2001) based their initial conditions on rawinsonde data from 12 weakly forced, warm-season, progressive derechos. These initial conditions are representative of the conditions present for the MCSs in the present study, which could explain why low-level shear values of Coniglio and Stensrud (2001) are more comparable to values of the present study than Weisman's (1992) low-level shear values. Evans and Doswell (2001) studied United States derechos from 1983 to 1993 and found the middle 50% of 0–2-km shear values ranging from 7 to 12 m s^{-1} for weakly forced derechos. Wind damage reports from *Storm Data* suggest that 15 of the 47 MCSs for the present study were classified as progressive derechos, most of which formed in weakly forced environments.

There are other differences between Weisman's (1992) simulations and the MCSs of the present study. Weisman's simulations are of a 4-h period beginning with convective initiation, a time period in the MCSs' life cycles sampled by just one-fourth of the cases for the present study. In addition, the resolution of observational data is not as fine as that used in the simulations. Because of this lack of fine resolution, the true cold

pool–shear balance occurring at the gust front often may not be sampled in the present study.

It is important to note that Rotunno et al. (1988, 1990), Weisman et al. (1988), and Weisman (1992) all are stating conditions for an optimal state, or conditions that lead to the strongest, longest-lived squall lines. The MCSs can be "out of balance," not in optimal states, and still survive for long periods of time with upshear-tilted updrafts. Their simulated MCSs achieve optimal states and are very strong linear systems, but after several hours, depending on how strong their 0–2.5-km shear is, the systems shift to less-than-optimal states with updrafts that become weaker and more upshear tilted with time. However, Coniglio and Stensrud's (2001) results suggest strong updrafts can be maintained for as many as 6 h at less-than-optimal states. The results of the present study tend to support Coniglio and Stensrud (2001), showing that MCSs do maintain their strength for long periods under less than optimal cold pool–shear balance ratios.

Recall the simulations of Weisman et al. (1988) with 0–2.5-km shear of 10 m s^{-1}. Their cold pool–shear balance ratio had a magnitude between 2 and 2.5 throughout the entire simulation, and they note, "This squall line weakened considerably after 1 h (as it tilted strongly upshear with time), and significant cell regeneration essentially stopped by 2 h." Many MCSs in the present study clearly did not behave in the manner of the simulations of Weisman et al. (1988). Even with cold pool–shear balance ratios of 3 or greater, strong convective lines maintained their strength for many hours and were even shown to increase in strength for some MCSs in the present study. This appears to contradict Rotunno et al. (1990) who state that an appropriate balance between the cold pool and the low-level line-normal shear is "a necessary requirement for sustaining most strong squall lines."

One last way to account for differences between the present study and Weisman (1992) is that Weisman's simulations were for surface-based convection. As has been noted earlier, there is evidence to suggest the majority of the present study's MCSs ingest more elevated inflow air than surface-based inflow air for at least a portion of their lifetimes, whether because the MCSs are north of boundaries, or because they are traveling through areas with low-level temperature inversions. When the situation arises where the base of the convection is elevated, the MCSs may not be affected much by the interaction between the cold pool circulation and the low-level shear circulation. Therefore, the cold pool's involvement in the continued generation of new convective cells would be minimal. The continued generation of new convective cells instead may be driven by mechanisms that may provide convergence near the base of the elevated convection such as gravity waves (Schmidt and Cotton 1990) or the LLJ (Bonner 1968).

The results of the present study agree with Coniglio and Stensrud (2001) in suggesting that the cold pool–
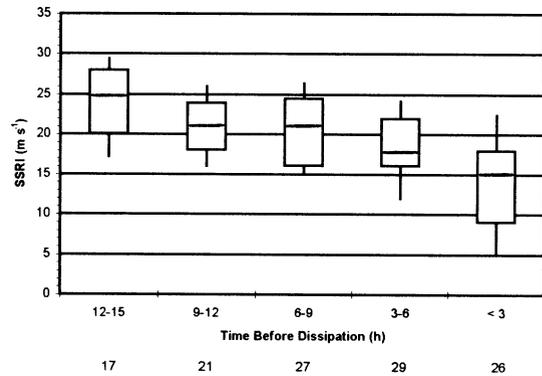

FIG. 5. As in Fig. 2 but for SSRI (m s^{-1}).

shear balance theory of Rotunno et al. (1998) and Weisman (1992) may be of little use to forecasters predicting MCS dissipation. For instance, since many MCSs of the present study maintain strong convection for long periods despite progressing in less-than-optimal states, it calls into question the usefulness of an "optimal" condition for forecasting the strength of long-lived squall lines. If the MCS is producing severe weather, a forecaster might not be interested in knowing if the MCS is optimal (i.e., producing the most severe weather it possibly could). Some of the highest cold pool–shear balance ratios recorded for the MCSs of the present study occurred while the MCSs' convective lines were approaching their most intense stages and were still many hours away from dissipation.

b. Surface system-relative inflow

System-relative inflow supplies ambient warm, moist, environmental air to a thunderstorm. This positively buoyant inflow air serves as a continuous stream of energy into the thunderstorm to help the thunderstorm sustain itself. A thunderstorm that has weak system-relative inflow, or whose inflow air is cool, may weaken or dissipate since it will not have enough energy to generate and maintain convection. The same reasoning may be applied to an MCS, but now the system-relative inflow is on a larger scale. If the system-relative inflow into the MCS is weak or weakens with time, it may be a factor in MCS dissipation.

1) GENERAL RESULTS

SSRI tends to decrease as dissipation approaches, especially in the 6 h prior to dissipation (Fig. 5). The decrease in the means is significant at the 90% confidence level between the 6–9- and 3–6-h before dissipation bin and at the 99% level between the 3–6-h and <3 h before dissipation bin. One way in which the box and whisker plots are useful is that they can help to gauge the value of a parameter in distinguishing among categories (Rasmussen and Blanchard 1998). Note from
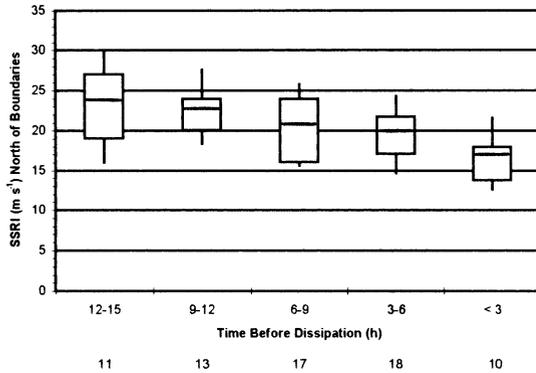
FIG. 6. As in Fig. 2 but for SSRI (m s^{-1}) of MCSs north of boundaries.
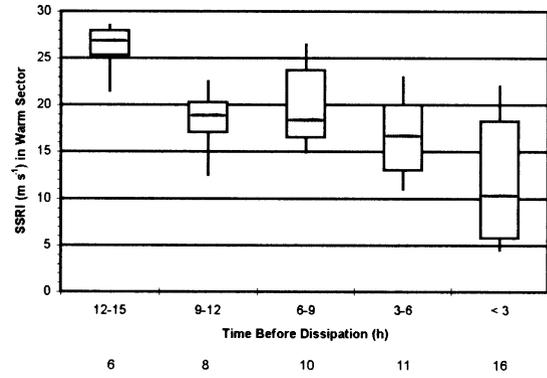

FIG. 7. As in Fig. 2 but for SSRI (m s^{-1}) of MCSs in warm sectors.

Fig. 5 that the median of the <3 h box lies outside the entire adjacent 3–6-h box. Rasmussen and Blanchard (1998) indicated that such a separation between values among bins is valuable in distinguishing between populations and should show the parameters with the best potential to assist forecasters. We can apply similar principles for the present study to state that the decrease seen in SSRI in the several hours before dissipation shows that SSRI has value as a potential predictor of MCS dissipation.

2) NORTH OF BOUNDARY VERSUS WARM SECTOR

MCSs occurring in the warm sector may be more likely to exhibit surface-based convection than MCSs occurring north of a boundary. Because of this possibility, the SSRI results in terms of time before dissipation were also divided into cases occurring in the warm sector and cases occurring north of a boundary. It is immediately evident from Fig. 6 that SSRI for north of boundary MCSs does not show a notable decrease until between 3–6 and <3 h hours before dissipation (the decrease is significant at the 90% confidence level). By comparison, Fig. 7 shows more erratic behavior of SSRI for warm sector MCSs early on, part of which could be due to small sample sizes. Later, large variability is present in the <3 h bin. However, the decrease in mean SSRI in the last 6 h before dissipation for warm sector cases (95% confidence) is greater than the corresponding decrease for north-of-boundary cases. Note also that all but one of the SSRI values of less than 10 m s^{-1} are found in warm sector cases. This indicates that SSRI may be more influential for warm sector cases than north-of-boundary cases, consistent with warm sector cases being more likely to exhibit surface-based convection for longer periods than north-of-boundary cases.

3) SURFACE WINDS

The trend for surface winds with time before dissipation is similar to the trend of SSRI with time before

dissipation (Fig. 8). Surface winds are highest 12–15 h before dissipation, but they stay relatively constant for the next 6 h before decreasing from 6–9 to <3 h before dissipation (99% confidence). However, the decreases in the means of surface winds are virtually unnoticeable (only a 1.3 m s^{-1} decrease from the 6–9-h mean to the <3 h mean). Thus, the trends in SSRI cannot be explained by surface winds. The MCS movement must play a significant role as well.

4) MCS MOVEMENT

MCS speed of movement more closely parallels the SSRI results. MCS movement is most rapid 12–15 h before dissipation and tends to stay steady until a noticeable decrease from 3–6 h to <3 h before dissipation that is significant at the 95% confidence level (Fig. 9). Note that there is a large amount of variability between cases. Some dissipated without showing a decrease in SSRI or MCS movement, a few showed an increase in the last 6 h before dissipation, while others showed a large decrease prior to the last 6 h before dissipation yet managed to survive the large decrease.

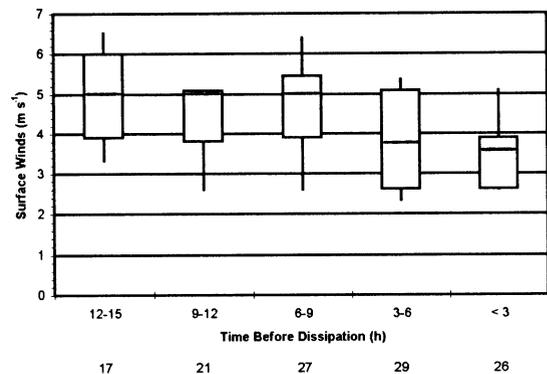One explanation for how the MCSs as a whole experience decreases in speed as dissipation nears could

FIG. 8. As in Fig. 2 but for average surface winds (m s^{-1}) taken from environments ahead of the MCSs.
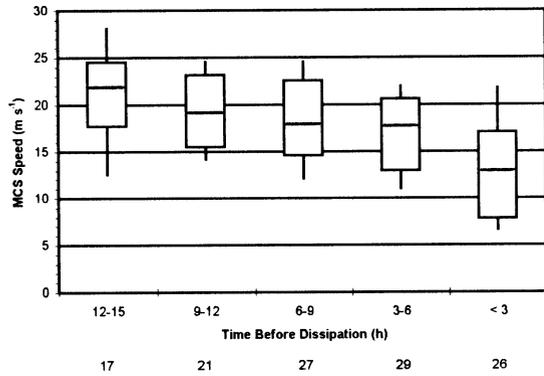
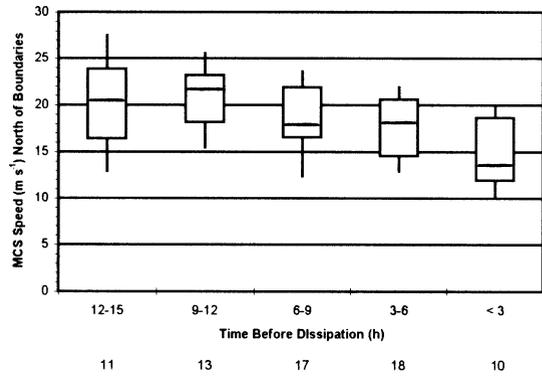Fig. 9. As in Fig. 2 but for MCS speed of movement (m s^{-1}).

Fig. 10. As in Fig. 2 but for speed of movement (m s^{-1}) of MCSs north of boundaries.

be due to a change in measurement of the MCS speed between convective lines and stratiform centroids. Convective lines are known to separate from the stratiform regions behind them (forming the transition zone) often as stratiform regions seem to slow down (Gallus and Johnson 1991). The slowing of the stratiform region may be due to the development of a midlevel circulation late in the MCS lifetime that induces more front-to-rear flow. In addition, the stratiform region may expand rearward with time, which could result in a slowing of forward speed when the stratiform centroid's position is used (Gallus and Johnson 1991).

Convective lines also may separate from the stratiform regions behind them if the convective lines themselves accelerate toward dissipation as the cold pool strength and descending rear-inflow jet increase to the point of overpowering the ambient shear (Gallus and Johnson 1991; Weisman 1992). At this stage, a gust front representing the front edge of the cold pool may surge ahead of the convective line. (Resolution of radar data used for the present study is not fine enough to resolve surging gust fronts, but during the summers of 2000 and 2001, higher-resolution real-time radar data sometimes showed gust fronts surging ahead of convective lines with a noticeable weakening in the convection becoming apparent an hour or two later).

In the present study, sometimes a slowing in MCS speed may result because of a switch from measuring the speed of the convective line for one 2-h period to measuring the speed of the stratiform centroid for the next 2-h period if convection had dissipated. Nonetheless, a slowing of the speed of the convective line itself is noted for many cases.

MCS movement was also compared between cases that occurred north of a boundary (Fig. 10) and cases in the warm sector (Fig. 11). Cases north of a boundary moved more rapidly (18.6 m s^{-1}), on average, than cases in the warm sector (16.0 m s^{-1}). This may be explained by noting cases north of boundaries probably occurred in regimes more baroclinic than those that occurred in warm sectors. Increased baroclinicity is positively cor-

related with higher wind speeds, which could lead to faster-moving MCSs.

c. Elevated system-relative inflow

The majority of the MCSs occurred north of a boundary. Low-level winds in the vicinities of the MCSs usually had significant southerly components, so that buoyant air serving as inflow to the MCSs originated south of the boundaries and had to rise over the boundaries in order to be drawn into the MCSs. Therefore, it is likely much of the inflow for MCSs north of boundaries is not surface based. In addition, though many of the 0000 UTC soundings do not show low-level temperature inversions, all 1200 UTC soundings show low-level temperature inversions for north-of-boundary cases, implying elevated convection overnight as the MCSs likely decouple from the surface and draw inflow air from lower levels just above the inversion layers (Cotton et al. 1989). In the previous section, it was shown that MCSs north of boundaries did not experience significant decreases in SSRI as they approached dissipation, while MCSs in the warm sector did, suggesting MCSs north of a boundary are less dependent on surface conditions than MCSs in the warm sector.
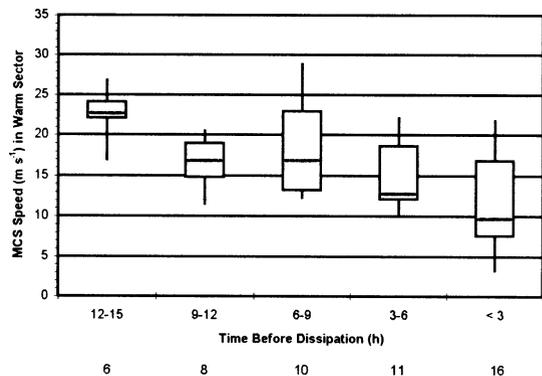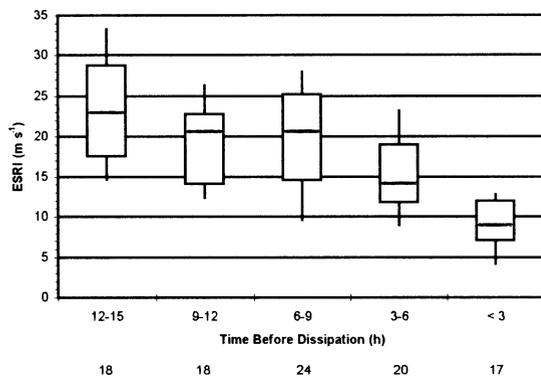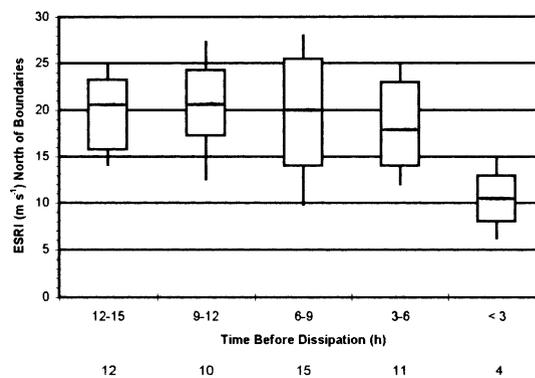

Fig. 11. As in Fig. 2 but for speed of movement (m s^{-1}) of MCSs in warm sectors.

FIG. 12. As in Fig. 2 but for ESRI (m s^{-1}).

FIG. 13. As in Fig. 2 but for ESRI (m s^{-1}) of MCSs north
of boundaries.

The tendency for the MCSs of the present study to occur north of boundaries and/or in environments consisting of low-level temperature inversions makes it necessary to calculate an elevated system-relative inflow (ESRI) in addition to a surface system-relative inflow.

1) GENERAL RESULTS

Average ESRI (figure not shown) is greatest at 0600 UTC (22.4 m s^{-1}) then decreases to its minimum at 1800 UTC (14.5 m s^{-1}). The large value at 0600 UTC most likely reflects the influence of the LLJ (see later LLJ discussion).

Figure 12 shows that with time before dissipation, ESRI is similar to SSRI, but the decrease as dissipation approaches is greater. ESRI is a maximum, on average, 12–15 h before dissipation. Average ESRI then decreases sharply from 6–9 h before dissipation to <3 h before dissipation. Note especially that the <3 h box is nearly entirely outside the 3–6-h box. The mean ESRI for the 3–6-h bin is 15.6 m s^{-1} and decreases to 8.6 m s^{-1} in the <3 h bin (significant at the 99% confidence level). Thus, the decrease in ESRI is considered significant as a predictor of MCS dissipation, even considering the large amount of variability in the data, and it appears to be more significant than SSRI.

2) NORTH OF BOUNDARY VERSUS WARM SECTOR

When the results of the ESRI calculation are broken down into cases in the warm sector and cases north of boundaries, there is a decrease in ESRI as dissipation approaches for both north-of-boundary (Fig. 13) and warm sector (Fig. 14) cases. However, the decrease is greater for warm sector cases.

For cases north of boundaries, Fig. 13 shows ESRI is greatest 12–15 h before dissipation. It stays fairly constant and decreases slightly as dissipation draws nearer before decreasing sharply from 3–6 h to <3 h before dissipation (95% confidence). Note, however, the small sample size of the <3 h bin, due both to cases dissipating 3 h or more after 1800 UTC and to cases

moving east of the wind profiler network well before dissipation.

For warm sector cases, there is greater variation in ESRI well before dissipation, as opposed to cases north of boundaries that exhibit nearly constant averages until the last 3 h before dissipation.

Figure 14 shows ESRI for warm sector cases is highest 12–15 h before dissipation. It then decreases sharply to the 9–12-h box, which is similar to the 6–9-h box. There is another sharp decrease between the 6–9- and 3–6-h boxes corresponding to a decrease in the means that is significant on the 99% confidence level. Note that the ESRI for warm sector cases begins its large decrease earlier than it does for cases north of boundaries. The <3 h box shows a further decrease from the 3–6-h box (95% confidence) for warm sector cases.

Earlier, it was noted that ESRI may be more important than SSRI for cases north of boundaries since those cases would likely exhibit predominantly elevated convection. Cases north of boundaries show a decrease in SSRI as dissipation approaches, but for ESRI the decrease is larger. These results suggest that a decrease in ESRI is more significant than SSRI as a predictor of dissipation for MCSs north of boundaries.

For warm sector cases, the decrease in ESRI in the
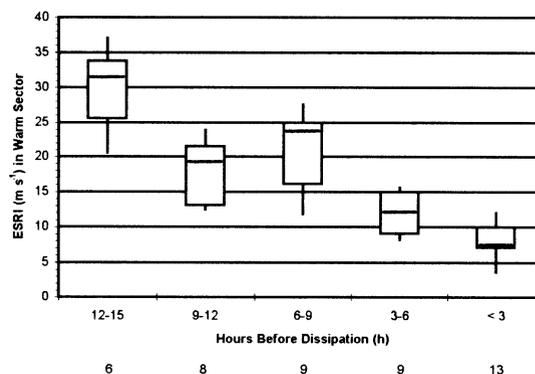
FIG. 14. As in Fig. 2 but for ESRI (m s^{-1}) of MCSs in
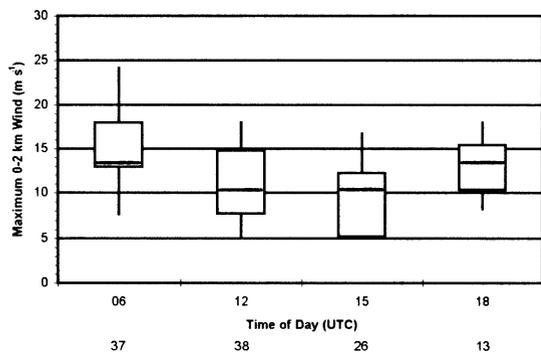warm sectors.

FIG. 15. As in Fig. 2 but for maximum 0–2-km wind speed (m s^{-1}) with time of day (UTC) taken from environments ahead of the MCSs.
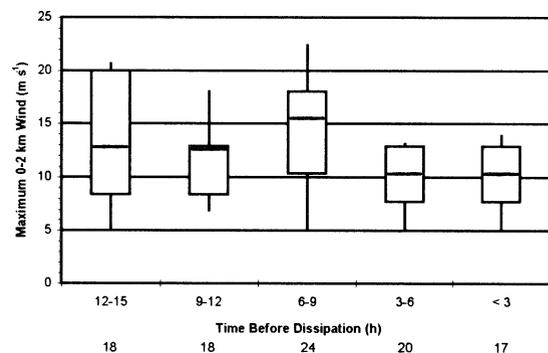

FIG. 16. As in Fig. 2 but for maximum 0–2-km wind speed (m s^{-1}) with time before dissipation (h) taken from environments ahead of the MCSs.

last 6–9 h before dissipation is greater than with SSRI. This may suggest that many warm sector cases draw inflow from above the surface whether they have surface-based convection or not. Also, nocturnal low-level temperature inversions often were present in 1200 UTC rawinsonde observations for warm sector cases as well as for north-of-boundary cases and may have caused the convection to be elevated for significant periods of time, thus increasing the influence of ESRI on the MCSs.

3) MAXIMUM 0–2-KM WIND

It was observed earlier for SSRI that MCS movement more closely parallels SSRI than the surface winds. For ESRI, the maximum 0–2-km winds were greater in magnitude than the surface winds and may have been more important to the calculation of ESRI than the surface winds were in the calculation of SSRI.

The maximum 0–2-km winds are strongest at 0600 UTC and weakest at 1500 UTC (Fig. 15). The high value at 0600 UTC is probably indicative of the presence of the LLJ. The decrease as the morning goes on is consistent with LLJ occurrences being less common at 1200 and 1500 UTC than at 0600 UTC (Bonner 1968; Mitchell et al. 1995; Arritt et al. 1997). The increase between 1500 and 1800 UTC could be representative of an increase in southerly wind events (SWEs). An SWE is different from an LLJ in that an SWE is not required to show a local maximum in the vertical profile of the wind speed. Arritt et al. (1997) found that non-LLJ SWEs are most likely in the Great Plains in the afternoon and early evening hours. The stronger maximum 0–2-km winds at 1800 UTC suggest that if an MCS can survive weaker ESRI through the morning hours and continue into the afternoon, it may have a good chance of sustaining itself for several more hours afterward because of increasing low-level winds.

With time before dissipation, average maximum 0–2-km winds behave similarly to surface winds in that there are not large differences between the mean values, but there is more variability in the maximum 0–2-km

winds (Fig. 16). However, there is a moderate decrease in maximum 0–2-km winds from 6–9 h to 3–6 h before dissipation (99% confidence).

Note that the value of the 6–9-h before dissipation median is highest, unlike most previous results studied that always have their highest medians in the 12–15-h before dissipation bin. There are a few exceptionally large values of maximum 0–2-km wind included in the 6–9-h bin that contribute to its higher median. These large values are from 0600 UTC and come from cases that experienced significant decreases in maximum 0–2-km winds between 0600 and 1200 UTC that may have contributed to their dissipation around or just after 1200 UTC. So the fact that the maximum 0–2-km winds have greater magnitudes and greater decreases as dissipation approaches than surface winds do helps to explain why ESRI decreases more than SSRI as dissipation approaches.

d. Low-level jet

Recall from section 2 that the LLJ data are for the months of June–August of 1998–99. This limits the LLJ dataset to 37 MCSs instead of 47. For 34 out of 37 cases, an LLJ affects the MCS during at least one of the four times examined (0600, 1200, 1500, or 1800 UTC). This suggests that it is rare for MCSs to propagate through Iowa and surrounding states through the night-time and morning hours without being affected by LLJs to some degree.

Low-level jets most commonly affect MCSs at 0600 UTC. There are LLJs affecting 28 out of 32 (or 87.5% of) ongoing MCSs at 0600 UTC. The percentage drops to 67% (23 out of 34) at 1200 UTC, and then it drops sharply to 27% (6 out of 22) at 1500 UTC and 11% (1 out of 9) at 1800 UTC. The LLJs are likely affecting MCSs most at 0600 UTC because it is a time when LLJs most commonly occur. Bonner (1968) found peak LLJ occurrence to be between 0600 and 1200 UTC; Mitchell et al. (1995) and Arritt et al. (1997) found peak LLJ occurrence to be between 0600 and 0900 UTC. The

results of the latter two studies also clearly show LLJ frequency to steadily decline from 1200 UTC through 1500 and 1800 UTC, in agreement with the present study's findings.

A stronger association is found to exist between MCS dissipation and the termination of the LLJ than between MCS dissipation and the weakening of the LLJ. There is a slight tendency for MCSs to dissipate after experiencing a decrease in the intensity of LLJs (i.e., progress from a criterion-3 LLJ to a criterion-2 LLJ) affecting them. For cases affected by LLJs for at least two consecutive time periods, 11 cases experience a decrease in LLJ intensity, 6 experience no change, and 4 experience an increase in LLJ intensity.

There is a stronger tendency for MCSs to not be affected by an LLJ less than 3 h before dissipation. Of 19 cases with measurements in that category that were previously affected by an LLJ, 13 are no longer affected by an LLJ. Thus, an LLJ does not necessarily have to be strong to potentially aid in the sustenance of an MCS. What may be most important regarding LLJs and MCS dissipation is either MCS movement too far from LLJs to continue being affected by them, or termination of LLJs affecting the MCSs, causing the MCSs to lose warm, moist air supplied by and convergence caused by the LLJs. Although MCSs generally do not survive the loss of the LLJ influence, there are exceptions. Likewise, some MCSs dissipate while still being affected by an LLJ. As is evident in the analysis of all parameters studied, MCS dissipation is quite complex, and no one parameter fully explains it.

e. Lapse rates and maximum 0–2-km θ_e

Forecasters often analyze the static stability of the atmosphere to predict severe weather. The initial thunderstorms that eventually develop into an MCS are often severe thunderstorms developing in environments of high conditional instability. Two ways for forecasters to gauge instability are low-level to midlevel lapse rates and low-level θ_e. As noted in the introduction, low-level θ_e has previously been documented as a possible factor in MCS development and sustenance (Cotton et al. 1989; Parker and Johnson 2000). Thus, it is expected that low-level θ_e and lapse rates may be factors in MCS dissipation.

1) LAPSE RATES

The surface–700-mb lapse rates decrease from 0000 to 1200 UTC (figure not shown), but the decrease is almost entirely due to the surface temperatures decreasing overnight, which happens every night.

The 850–500- and 700–500-mb layer lapse rates usually decrease only slightly from 0000 to 1200 UTC (figure not shown). A forecaster would pay little attention to a lapse rate decrease of 1 or 2 K from 0000 to 1200 UTC. However, a potentially useful forecasting tool was

found for a small number of cases that experience a decrease in the 850–500-mb lapse rate of 5 K or greater from 0000 to 1200 UTC. These cases tend to dissipate around 1200 UTC. Out of nine cases that experience a decrease in the 850–500-mb lapse rate of 5 K or greater, six dissipated by or before 1500 UTC, and two dissipated by 1900 UTC. Thus, a decrease of 5 K or more between 0000 and 1200 UTC from soundings ahead of the MCS strongly indicates that the MCS will dissipate at a relatively early time.

Similar to the 850–500-mb lapse rate, the cases that experience a decrease of 5 K or more in the 700–500-mb lapse rate tend to dissipate around 1200 UTC. Four of the six cases that experience a decrease of 5 K or more dissipate by 1300 UTC, and the remaining two dissipate by 1800 UTC. The four cases dissipating by 1300 UTC are also four of the cases that experience a decrease of 5 K or more for the 850–500-mb layer. The lapse rates for these four cases decrease by such a large amount primarily because of cooler temperatures at 850 and 700 mb, while the 500-mb temperature remains nearly constant.

It appears that lapse rates generally do not change significantly as MCSs progress. However, somewhat rare cases that experience larger-than-average decreases in the 850–500- and 700–500-mb lapse rates tend to dissipate by or very soon after 1200 UTC, suggesting forecasters should monitor these lapse rates as the MCSs progress.

2) MAXIMUM 0–2-KM θ_e

The maximum 0–2-km θ_e decreases by 9.6 K from 0000 to 1200 UTC (figure not shown). Although this decrease of 9.6 K seems substantial, there is much variability in the data. The standard deviations of the data are greater than 10 K, meaning that the average values at 0000 and 1200 UTC are within one standard deviation of each other. In addition, the average value at 1200 UTC is 339.1 K. In general, the θ_e values at 1200 UTC from 2 to 5 km AGL are lower than the 0–2-km maximum, implying the MCSs are still moving into conditionally unstable environments at 1200 UTC. The sounding used by Rotunno et al. (1988) and Weisman (1992) to represent the initial environments of their squall line simulations had a maximum low-level θ_e value of 338.2 K. Most MCSs in the present study moved through environments of maximum 0–2-km θ_e values greater than 338 K.

The highest maximum 0–2-km θ_e value (378 K) occurred at 0000 UTC for an MCS on 3 July 1999. By 1200 UTC, the maximum 0–2-km θ_e had decreased markedly to 340 K, yet the convective line associated with the MCS was at its most intense and well-organized stage at this time. However, a few hours later, the line had weakened, and the system dissipated by 1900 UTC. It does appear for this case, and several others, that once the MCS moved into the environment of much lower

maximum 0–2-km θ_e, it weakened. Yet, other cases experienced similar decreases in maximum 0–2-km θ_e and did not dissipate soon afterward.

On 21 May 1998, the maximum 0–2-km θ_e at 0000 UTC was 358 K. At 1200 UTC, it was 324 K, one of the lowest values observed. Yet, the MCS did not develop until 0900 UTC, and it sustained itself for 21 h, all the way to 0600 UTC on 22 May (note that for cases that had not developed by 0000 UTC, the soundings used to calculate the lapse rates and maximum 0–2-km θ_e were from areas within 300 km of where the first storms of the MCSs later developed). Similarly, of cases that experienced little change in maximum 0–2-km θ_e between 0000 and 1200 UTC, some dissipated soon after 1200 UTC, while others continued to progress for 10 or more hours.

It is evident that maximum 0–2-km θ_e and the rate of change of maximum 0–2-km θ_e alone do not explain the dissipating behaviors of MCSs. However, sometimes a large decrease in maximum 0–2-km θ_e may be one of many factors contributing to MCS dissipation. In general, though, the MCSs for the present study are moving through conditionally unstable environments with ample maximum 0–2-km θ_e available to them at or near the times in which they dissipate, which makes it very difficult to use maximum 0–2-km θ_e to predict MCS dissipation.

f. Eta Model results

Thus far, discussion has centered on observational data parameters that may aid the forecasting of MCS dissipation in real time. To calculate these observational parameters, the MCS has to be ongoing, and a forecaster's prediction of its dissipation probably can only be relayed to the public through short-term forecasts. It is desirable to reasonably predict MCS dissipation greater than just a few hours in advance of dissipation, or even before the MCS develops. If there are parameters within a numerical model, like the Eta, that could aid a forecaster in the prediction of MCS dissipation, then the Eta could be used to predict MCS dissipation further in advance than possible with observational data.

A forecaster can refer to the Eta precipitation output to aid in prediction of MCS dissipation, but since warm-season precipitation forecast skill scores are particularly poor, possibly due to deficiencies in precipitation generation within parameterizations, it is desirable to find other parameters that may be important for MCS dissipation as well. Recall from section 2 that the Eta Model parameters examined include wind speed, convergence, moisture convergence, frontogenesis, θ_e and θ_e advection at 850 mb for all, 500-mb vorticity advection, and 250-mb divergence. Most of these parameters show little or no potential as predictors of MCS dissipation in the Eta Model, with the exception of 850-mb θ_e advection, which shows moderate potential. Further discussion will therefore focus on 850-mb θ_e advection.
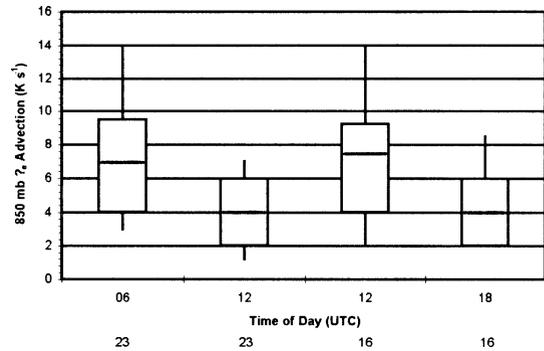

FIG. 17. As in Fig. 2 but for maximum 850-mb θ_e advection (1×10^{-4} K s^{-1}) with time of day (UTC) for Eta MCSs dissipating before 1800 UTC (the left two boxes) and Eta MCSs dissipating after 1800 UTC (the right two boxes).

Figure 17 shows that 850-mb θ_e advection decreases both from 0600 to 1200 UTC for cases dissipating before 1800 UTC (99% confidence) and from 1200 to 1800 UTC for cases dissipating after 1800 UTC (<90% confidence). Note that 1200 UTC values for earlier-dissipating cases are generally lower than 1200 UTC values for later-dissipating cases (95% confidence). In addition, larger values of 850-mb θ_e advection at 1200 UTC may suggest longer-lasting MCSs in the Eta Model. One-half of the 1200 UTC values for later-dissipating cases are 8.0×10^{-4} K s^{-1} or greater, while just 2 of 23 values for earlier-dissipating cases are 8.0×10^{-4} K s^{-1} or greater.

It should also be noted that the maximum 850-mb θ_e advection "bull's-eye" in the Eta Model often occurs in an area closer to the observed MCS than to where the Eta Model MCS occurs (figure not shown). Therefore, even if the Eta Model may not correctly forecast the MCS, a forecaster may still be able to use the model's output for 850-mb θ_e advection.

4. Conclusions

In the present study, observations and model output were examined to determine potential predictors of MCS dissipation. The dataset included 47 nocturnal MCSs that occurred during May–August 1998–99 in Iowa and surrounding states. Over 90% of the MCSs exhibited linear convective echo patterns for at least small portions of their lifetimes. The average duration of the MCSs was 19 h from first storms to light to moderate stratiform rain remnants.

The cold pool–shear balance theory of Rotunno et al. (1988) and Weisman (1992) was tested with observations but did not appear to correlate well with MCS dissipation. The cold pool–shear balance ratio is greater than 2 much more often than not, implying the cold pool circulation is overpowering the low-level shear circulation, and the MCSs are progressing in less-than-optimal states. Yet, many MCSs maintained strong con-

vection and progressed for many hours despite being in less-than-optimal states.

Discussion focused on interpretation of the cold pool–shear balance results. Low-level line-normal shear for our MCSs was almost one-third the magnitude of Weisman's (1992) moderate-shear simulation and one-fifth Weisman's strong-shear simulation. Our lower shear values explained why our balance values were so high. Discussion then turned to differences between Weisman's assumptions and our MCSs. Weisman assumed uniform winds above 2.5 km, which may be one reason why his 0–2.5-km line-normal shear must be so strong to maintain erect updrafts. Coniglio and Stensrud (2001) simulated a progressive derecho but allowed for deep-tropospheric shear and found that though the low-level shear was less than that of Weisman (1992), and the MCS was progressing in a less-than-optimal state, the MCS maintained strong updrafts above the gust front and did not weaken for over 6 h. More recent work by Weisman and Rotunno (2001) has included deep-tropospheric shear in squall line simulations. Results indicate squall lines can achieve optimal states with cold pool–shear balance ratios greater than 1 when deep-tropospheric shear is present as well as strong low-level shear. Deep-tropospheric shear was examined for 10 of our cases, and though there was much variability in the shear, winds above the low levels were certainly not uniform in the MCSs in the present study.

Other differences between our MCSs and Weisman's (1992) simulations that may help to explain why our results are different from the simulations include the following.

- Weisman's simulations were for a 4-h period beginning with convective initiation, while data were analyzed for our MCSs over a 12-h period beginning more than 6 h after convection initiated for the majority of the MCSs.
- The resolution of observational data is not as fine as that used in Weisman's simulations. Because of this lack of fine resolution, the true cold pool–shear balance occurring at the gust front often may not be sampled in the present study.
- The cold pool–shear balance theory is based on an optimal state for strong, long-lived squall lines. MCSs from the present study appear to maintain strong convection for long periods in less-than-optimal states with upshear-tilted updrafts. Thus, the MCS need not be ''optimal'' in order to be strong and long-lived.
- A significant number of our MCSs were smaller linear systems forming in environments of weaker low-level shear, than the large squall lines simulated in Rotunno et al. (1988) and Weisman (1992).
- Rotunno et al. and Weisman simulated surface-based convection, while the majority of our MCSs may have exhibited elevated convection due to being north of boundaries and/or in environments consisting of nocturnal low-level temperature inversions. The lift generated along any gust fronts may not have as much effect on the convection.

There are other parameters studied that do seem to be a factor in MCS dissipation. They include both surface (SSRI) and elevated (ESRI) system-relative inflow. Decreases in both SSRI and ESRI are associated with MCS dissipation. The decrease in SSRI as dissipation approaches is due mostly to a decrease in the MCS speed of movement. For ESRI, there is a greater decrease as dissipation approaches because the maximum 0–2-km wind tends to decrease in concert with MCS speed of movement.

MCSs north of boundaries tend to move faster than warm sector MCSs (likely in part due to increased baroclinicity north of boundaries), and they also tend to last longer. In addition, MCSs north of boundaries do not experience decreases in SSRI as large as warm sector MCSs do as dissipation approaches. For ESRI, though, the decreases as dissipation approaches for MCSs north of boundaries are more comparable to the decreases in ESRI for warm sector cases. However, MCSs north of boundaries do not experience a significant decrease in ESRI until within 3–6 h of dissipation, while warm sector cases experience a significant decrease between 6–9 and 3–6 h before dissipation. Thus it seems MCSs north of boundaries may last longer because they move faster on average, and therefore have greater average SSRI and ESRI, than MCSs in the warm sector. MCSs north of boundaries may also not be as dependent on SSRI as warm sector cases since they likely exhibit elevated convection, which can explain why they dissipate without significant reductions in SSRI.

The LLJ also appears to play a role in MCS dissipation. Over 90% of the MCSs were affected by an LLJ at some time. LLJs most commonly affect the MCSs at 0600 and 1200 UTC. Very few MCSs are affected by LLJs at 1500 and 1800 UTC, time periods when the majority of MCSs are dissipating or have dissipated. There is a slight tendency for MCSs to dissipate after experiencing a decrease in the intensity of LLJs affecting them. There is a greater tendency for MCSs to dissipate after LLJs that were once affecting them either terminate or are no longer affecting the MCSs because the MCSs moved too far away from them.

Instability parameters such as maximum 0–2-km θ_e and lapse rates in the low to midlevels do not appear to play major roles in MCS dissipation, except in rare cases. Lapse rates do not decrease significantly, in general. However, somewhat rare cases that experience larger-than-average decreases of 5 K or more in the 850–500- and 700–500-mb lapse rates tend to dissipate by or very soon after 1200 UTC. Maximum 0–2-km θ_e does decrease on average by almost 10 K from 0000 to 1200 UTC. However, most MCSs are moving through environments of maximum 0–2-km θ_e greater than 338 K at both 0000 and 1200 UTC. Rotunno et al. (1988) and Weisman (1992) initialize their simulations with a maximum low-level θ_e value of 338.2 K, so most of our

MCSs are experiencing maximum 0–2-km θ_e greater than that of their simulations throughout the MCSs' life cycles. Sometimes MCSs experience very large decreases in maximum 0–2-km θ_e and dissipate soon afterward. Other times they experience large decreases in maximum 0–2-km θ_e and continue propagating for many more hours.

Most Eta Model parameters studied show little or no potential as predictors of MCS dissipation, with the exception of 850-mb θ_e advection, which shows moderate potential. Lower 1200 UTC values of 850-mb θ_e advection suggest earlier dissipating Eta Model MCSs than higher 1200 UTC values suggest.

It is evident from the present study that MCS dissipation is very complex and difficult to predict, likely because of the large amount of variability between MCSs. There is still much to be understood, and much more research is needed in this area. The results of the present study are considered preliminary; larger datasets from wider geographical and climatological domains are needed. However, to aid prediction of MCS dissipation forecasters are encouraged to 1) examine SSRI and ESRI, paying particular attention to the MCS speed of movement; 2) distinguish between MCSs exhibiting elevated convection (those north of boundaries and/or in environments of low-level temperature inversions) and MCSs exhibiting surface-based convection (those in warm sector environments lacking low-level temperature inversions); 3) pay special attention to the LLJ to note whether it is influencing the MCS; and 4) examine low- to midlevel lapse rates looking for instances when they show significant decreases over time.

REFERENCES

Anderson, C. J., and R. W. Arritt, 1998: Mesoscale convective complexes and persistent elongated convective systems over the United States during 1992 and 1993. *Mon. Wea. Rev.,* **126,** 578–599.

Arritt, R. W., T. D. Rink, M. Segal, D. P. Todey, C. A. Clark, M. J. Mitchell, and K. M. Labas, 1997: The Great Plains low-level jet during the warm season of 1993. *Mon. Wea. Rev.,* **125,** 2176–2192.

Augustine, J. A., and K. W. Howard, 1988: Mesoscale convective complexes over the United States during 1985. *Mon. Wea. Rev.,* **116,** 685–701.

——, and ——, 1991: Mesoscale convective complexes over the United States during 1986 and 1987. *Mon. Wea. Rev.,* **119,** 1575–1589.

——, and F. Caracena, 1994: Lower-tropospheric precursors to nocturnal MCS development over the central United States. *Wea. Forecasting,* **9,** 115–135.

Bonner, W. D., 1968: Climatology of the low-level jet. *Mon. Wea. Rev.,* **96,** 833–850.

Coniglio, M. C., and D. J. Stensrud, 2001: Simulation of a progressive derecho using composite initial conditions. *Mon. Wea. Rev.,* **129,** 1593–1616.

Cotton, W. R., M.-S. Lin, R. L. McAnelly, and C. J. Tremback, 1989: A composite model of mesoscale convective complexes. *Mon. Wea. Rev.,* **117,** 765–783.

Evans, J. S., and C. A. Doswell III, 2001: Examination of derecho environments using proximity soundings. *Wea. Forecasting,* **16,** 329–342.

Fritsch, J. M., R. J. Kane, and C. R. Chelius, 1986: The contribution of mesoscale convective weather systems to the warm-season precipitation of the United States. *J. Climate Appl. Meteor.,* **25,** 1333–1345.

Gallus, W. A., Jr., and R. H. Johnson, 1991: Heat and moisture budgets of an intense midlatitude squall line. *J. Atmos. Sci.,* **48,** 122–146.

Janjic, Z. I., 1994: The step-mountain eta coordinate model: Further developments of the convection, viscous sublayer, and turbulence closure schemes. *Mon. Wea. Rev.,* **122,** 928–945.

Maddox, R. A., 1980: Mesoscale convective complexes. *Bull. Amer. Meteor. Soc.,* **61,** 1374–1387.

——, and B. E. Heckman, 1982: The impact of mesoscale convective weather systems upon MOS temperature guidance. Preprints, *Ninth Conf. on Weather Forecasting and Analysis,* Seattle, WA, Amer. Meteor. Soc., 214–218.

——, D. M. Rodgers, and K. W. Howard, 1982: Mesoscale convective complexes over the United States during 1981—Annual summary. *Mon. Wea. Rev.,* **110,** 1501–1514.

McAnelly, R. L., and W. R. Cotton, 1989: The precipitation life cycle of mesoscale convective complexes over the central United States. *Mon. Wea. Rev.,* **117,** 784–808.

Mesinger, F., Z. I. Janjic, S. Nickovic, D. Gavrilov, and D. G. Deaven, 1988: The step mountain coordinate: Model description and performance for cases of alpine cyclogenesis and for a case of an Appalachian redevelopment. *Mon. Wea. Rev.,* **116,** 1493–1518.

Mitchell, M. J., R. W. Arritt, and K. Labas, 1995: A climatology of the warm season Great Plains low-level jet using wind profiler observations. *Wea. Forecasting,* **10,** 576–591.

Parker, M. D., and R. H. Johnson, 2000: Organizational modes of midlatitude mesoscale convective systems. *Mon. Wea. Rev.,* **128,** 3413–3436.

Rasmussen, E. N., and D. O. Blanchard, 1998: A baseline climatology of sounding-derived supercell and tornado forecast parameters. *Wea. Forecasting,* **13,** 1148–1164.

Rodgers, D. M., K. W. Howard, and E. C. Johnston, 1983: Mesoscale convective complexes over the United States during 1982. *Mon. Wea. Rev.,* **111,** 2363–2369.

——, M. J. Magnano, and J. H. Arns, 1985: Mesoscale convective complexes over the United States during 1983. *Mon. Wea. Rev.,* **113,** 888–901.

Rotunno, R. J., B. Klemp, and M. L. Weisman, 1988: A theory for strong, long-lived squall lines. *J. Atmos. Sci.,* **45,** 463–485.

——, ——, and ——, 1990: Comments on "A numerical investigation of the organization and interaction of the convective and stratiform regions of tropical squall lines." *J. Atmos. Sci.,* **47,** 1031–1033.

Schmidt, J. M., and W. R. Cotton, 1990: Interactions between upper and lower tropospheric gravity waves on squall line structure and maintenance. *J. Atmos. Sci.,* **47,** 1205–1222.

Smull, B. F., and R. A. Houze Jr., 1987: Rear inflow in squall lines with trailing stratiform precipitation. *Mon. Wea. Rev.,* **115,** 2869–2889.

Stensrud, D. J., G. S. Manikin, E. Rogers, and K. E. Mitchell, 1999: Importance of cold pools to NCEP mesoscale Eta Model forecasts. *Wea. Forecasting,* **14,** 650–670.

——, J.-W. Bao, and T. T. Warner, 2000: Using initial condition and model physics perturbations in short-range ensemble simulations of mesoscale convective systems. *Mon. Wea. Rev.,* **128,** 2077–2107.

Weisman, M. L., 1992: The role of convectively generated rear-inflow jets in the evolution of long-lived mesoconvective systems. *J. Atmos. Sci.,* **49,** 1826–1847.

——, and R. Rotunno, 2001: The role of low-level vertical wind shear in promoting strong long-lived squall lines. Preprints, *Ninth Conf. on Mesoscale Processes,* Fort Lauderdale, FL, Amer. Meteor. Soc., 298–302.

——, J. B. Klemp, and R. Rotunno, 1988: Structure and evolution of numerically simulated squall lines. *J. Atmos. Sci.,* **45,** 1990–2013.